

# HIAPER Pole-to-Pole Observations (HIPPO): fine-grained, global-scale measurements of climatically important atmospheric gases and aerosols

BY S. C. WOFSY\*, THE HIPPO SCIENCE TEAM  
AND COOPERATING MODELLERS AND SATELLITE TEAMS†

*Harvard University, Cambridge, MA, USA*

The HIAPER Pole-to-Pole Observations (HIPPO) programme has completed three of five planned aircraft transects spanning the Pacific from 85° N to 67° S, with vertical profiles every approximately 2.2° of latitude. Measurements include greenhouse gases, long-lived tracers, reactive species, O<sub>2</sub>/N<sub>2</sub> ratio, black carbon (BC), aerosols and CO<sub>2</sub> isotopes. Our goals are to address the problem of determining surface emissions, transport strength and patterns, and removal rates of atmospheric trace gases and aerosols at global scales and to provide strong tests of satellite data and global models. HIPPO data show dense pollution and BC at high altitudes over the Arctic, imprints of large N<sub>2</sub>O sources from tropical lands and convective storms, sources of pollution and biogenic CH<sub>4</sub> in the Arctic, and summertime uptake of CO<sub>2</sub> and sources for O<sub>2</sub> at high southern latitudes. Global chemical signatures of atmospheric transport are imaged, showing remarkably sharp horizontal gradients at air mass boundaries, weak vertical gradients and inverted profiles (maxima aloft) in both hemispheres. These features challenge satellite algorithms, global models and inversion analyses to derive surface fluxes. HIPPO data can play a crucial role in identifying and resolving questions of global sources, sinks and transport of atmospheric gases and aerosols.

**Keywords:** monitoring; polar; atmospheric science

## 1. Introduction

Future action on climate change requires us to be able to distinguish surface emissions of greenhouse gases (GHGs) directly associated with human activities from indirect effects of climate change and from natural variations. Measurements of concentrations of GHGs (e.g. CO<sub>2</sub>, CH<sub>4</sub> and N<sub>2</sub>O) and tracers (e.g. CO, SF<sub>6</sub>, O<sub>2</sub>/N<sub>2</sub>) have been used to derive surface fluxes, and to attribute emissions to human activity or natural processes, in a variety of conceptual frameworks [1–6]. A common approach is to exercise atmospheric chemistry transport models (ACTMs) to simulate concentrations of pollutants in time and space over the globe, typically combining *a priori* surface emission flux fields, rates for chemical

\*Author for correspondence ([wofsy@fas.harvard.edu](mailto:wofsy@fas.harvard.edu)).

One contribution of 17 to a Discussion Meeting Issue ‘Greenhouse gases in the Earth system: setting the agenda to 2030’.

reactions in the atmosphere and assimilated meteorological fields. The surface flux field is then adjusted to obtain the best match between model output and data. The model is effectively ‘inverted’ to define optimal sources and sinks from atmospheric concentrations.

Global-scale ACTMs have difficulty resolving sharp chemical gradients, such as exist at air mass boundaries, at the tropopause [7,8] or in plumes of tracers emanating from strong source regions, a limitation inherent in the numerical methods used in the Eulerian model framework [9]. ACTM outputs are commonly compared with datasets that likewise do not resolve sharp gradients or define fine-scale variance and covariance, e.g. data from sparse ground stations or satellites. These data are in some respects ideal for comparison with global simulations, since they may be presumed to represent large air masses and global-scale processes. But, because accurate knowledge of vertical and horizontal gradients is available neither from global data nor from global models, the fine-grained structure of atmospheric tracer distributions is unknown and we have no way to assess how important this structure might be for inverse models.

Air mass boundaries move in space and time. Spatially aggregated data, or measurements from widely spaced locations (e.g. remote island stations), give horizontal patterns with diffuse boundaries. This fuzzy picture might be correct if data are averaged over time (e.g. for a month), but the pattern is never actually present in the atmosphere. A model may reproduce these smoothed gradients with simulated rates of transport across air mass boundaries that are significantly in error, leading to incorrect surface fluxes inferred from an inverse analysis. Similarly, if the vertical gradient in a model is systematically in error, the atmospheric mass burden (or column integral) is improperly simulated, and significant bias can result when the model is inverted to obtain optimal surface fluxes (e.g. [10]).

Surface fluxes obtained by inverting global models are also subject to systematic errors derived from other elements of the model framework, in addition to transport errors. For example, misidentification of source processes and locations, or incorrectly specified temporal variation of *a priori* fluxes, introduces errors into ‘optimal’ flux fields associated directly with model constructs. Since generally the only adjustable parameters in an inverse model are surface fluxes, strong, independent tests of all elements of the model framework are needed, using atmospheric measurements, in order to reduce the impact of these diverse systematic errors and biases.

This paper introduces the data obtained by the HIAPER Pole-to-Pole Observations (HIPPO) project, a sequence of five global aircraft measurement programmes that sample the atmosphere from (almost) the North Pole to the coastal waters of Antarctica, from the surface to 14 km, spanning the seasons. Three have been completed to date—January and November 2009, April 2010—to be followed by June and August/September 2011 (denoted HIPPO-1, -2, etc.). This paper will focus primarily on results obtained in HIPPO-1, for which data have been finalized.

HIPPO is intended to obtain global-scale, fine-grained data for the first time, for a large number of atmospheric constituents. HIPPO data provide high-resolution, systematic, pole-to-pole curtains with deeper vertical extent than possible in the past, acquired at high temporal resolution to preserve correlations among constituents. The goal is to provide new perspectives on how to use data

to wring out transport issues in ACTMs, to identify and address the errors in the spatial/temporal representation of surface fluxes and reaction rates, to discover new features of trace gas and aerosol emissions and global-scale transport and to rigorously test satellite algorithms. A related goal is to elucidate the underlying processes and controls on surface emission fluxes, in order to be able to predict emissions and atmospheric concentrations in the future.

Fine-grained data have been obtained previously from aircraft platforms, but only a few datasets have long transects covering extended time periods, principally from commercial airliners that acquire data exclusively at cruise altitude plus vertical profiles entering/leaving large urban complexes [11–13]. High-resolution datasets spanning the depth of the atmosphere over large areas are available from a few surveys [14–17] that covered much smaller domains and seasonal intervals than HIPPO. Thus, HIPPO data provide hitherto unavailable information for testing and refining understanding of global distributions and surface fluxes of trace gases and aerosols.

## 2. HIAPER Pole-to-Pole Observations payload

HIPPO measurements are summarized in table 1. The platform is the National Science Foundation's Gulfstream V (GV or HIAPER) aircraft operated by the National Center for Atmospheric Research (NCAR). Major GHGs ( $\text{CO}_2$ ,  $\text{CH}_4$ ,  $\text{N}_2\text{O}$ ) and other important trace species ( $\text{CO}$ ,  $\text{SF}_6$ ,  $\text{O}_2/\text{N}_2$ ,  $\text{H}_2$ , etc.) were measured at high frequency, many at 1 Hz, with two (or more) independent measurements for each to provide redundancy (five for  $\text{CO}_2$ ), check calibration and assess sensor drift. The quantum cascade laser spectrometer (QCLS), which measures  $\text{CO}_2$ ,  $\text{CO}$ ,  $\text{CH}_4$  and  $\text{N}_2\text{O}$ , is a mid-infrared (IR) sensor developed by Harvard University and Aerodyne Corp., owned by NCAR, and operated during HIPPO by the Harvard team; the Observations of the Middle Stratosphere (OMS) is a Harvard  $\text{CO}_2$  sensor using an IR gas analyser (IRGA), which has logged more than 300 flights on airborne platforms [18]. The Research Aviation Facility CO monitor (RAF-CO) refers to NCAR's AeroLaser AL5002 vacuum-UV sensor. Data at 1 Hz were obtained in two independent measurements for  $\text{O}_3$  and for  $\text{H}_2\text{O}$  (by the Vertical Cavity Surface Emitting Laser (VCSEL), a new open path near-IR multi-pass spectrometer [19], and by the Unmanned Aircraft Systems (UAS) Chromatograph for Atmospheric Trace Species (UCATS)- $\text{H}_2\text{O}$ , a National Oceanic and Atmospheric Administration (NOAA) mid-IR spectrometer with a sampling inlet). AO2 is the NCAR Airborne Oxygen Instrument, which measures  $\text{O}_2$  using a vacuum-UV absorption technique [20] and  $\text{CO}_2$  using a single-cell IRGA (Licor 850). UCATS and the PAN (PeroxyAcylNitrate) and other Trace Hydrohalocarbon Experiment (PANTHER) are on-board gas chromatographs with extensive flight histories, measuring at 1–3 min intervals.

A comprehensive suite of GHGs and a diverse ensemble of halocarbons, hydrocarbons and sulphur species were measured by the whole-air sampler system (WAS; [8]), using three different collection systems: stainless steel electropolished cylinders (the Advanced Whole Air Sampler (AWAS) from the University of Miami), glass vessels from the NOAA Programmable Flask Package (PFP) programme (NWAS from NOAA) and special glass vessels for measuring  $\text{O}_2/\text{N}_2$

Table 1. Measurements and species on the GV in HIPPO. Bold font indicates species with three or more measurements, sampling rates in parentheses.

Harvard/Aerodyne—HAIS QCLS	<b>CO<sub>2</sub></b> , <b>CH<sub>4</sub></b> , <b>CO</b> , <b>N<sub>2</sub>O</b> (1 Hz)
NCAR AO2	O <sub>2</sub> /N <sub>2</sub> , <b>CO<sub>2</sub></b> (0.5 Hz)
Harvard OMS CO <sub>2</sub>	<b>CO<sub>2</sub></b> (0.5 Hz)
NOAA CSD O <sub>3</sub>	O <sub>3</sub> (1 Hz)
NOAA GMD O <sub>3</sub> , H <sub>2</sub> O	O <sub>3</sub> , H <sub>2</sub> O (1 Hz)
NCAR RAF-CO	<b>CO</b> (1 Hz)
NOAA UCATS and PANTHER gas chromatographs	<b>CO</b> , <b>CH<sub>4</sub></b> , <b>N<sub>2</sub>O</b> , CFCs, HCFCs, <b>SF<sub>6</sub></b> , CH <sub>3</sub> Br, PAN, CH <sub>3</sub> Cl, H <sub>2</sub> , H <sub>2</sub> O (1 sample per 70–200 s)
whole-air sampling: NWAS (NOAA), AWAS (Miami), MEDUSA (NCAR/Scripps)	O <sub>2</sub> /N <sub>2</sub> , N <sub>2</sub> /Ar, <b>CO<sub>2</sub></b> , <b>CH<sub>4</sub></b> , <b>CO</b> , <b>N<sub>2</sub>O</b> , other GHGs, halocarbons, <b>SF<sub>6</sub></b> , H <sub>2</sub> , COS, CS <sub>2</sub> , solvent gases, reactive hydrocarbons, marine species, isotopes of CO <sub>2</sub> , etc.
VCSSEL Princeton/SWS	H <sub>2</sub> O (1 Hz)
NOAA SP2	BC mass, size (1 Hz)
MTP, wing stores	T, P, vertical structure, winds, aerosols, cloud water

and Ar/N<sub>2</sub> ratios and the isotopic composition of CO<sub>2</sub> (Multiple Enclosure Device for Unfractionated Sampling of Air (MEDUSA) from the University of California at San Diego).

BC was measured at 1 Hz by the NOAA single-particle soot photometer (SP2) [21] on air drawn into the cabin. The SP2 uses a laser beam to heat the BC component of individual fine-mode aerosol particles to vaporization, resulting in emission of thermal radiation that is interpreted to give the BC mass concentration and size distribution. Other particle probes, including a cloud droplet probe (CDP), the NCAR Ultra High Sensitivity Aerosol Sampler (UHSAS), the 2D-C particle imager and the PMS liquid water sensor (King) (Precipitable Liquid Water Content (PLWC)), resided on the wing, along with the microwave temperature profiler (MTP), which measures the temperature profile above and below the plane, and a digital camera that acquired an image every second.

### 3. Results

Figure 1 shows the flight tracks for HIPPO-1 and -2, plus vertical sampling and observed isentropic structure for HIPPO-1. Each deployment obtained a southbound cross section of the atmosphere near the International Date Line, covering the Arctic Ocean, Alaska and the entire Pacific to just short of Antarctica. Northbound, HIPPO-1 traversed the South Pacific to sample in the eastern tropical Pacific upwelling zone, and HIPPO-2 sampled the western Pacific warm pool. We obtained 138, 151 and 136 vertical profiles in HIPPO-1, -2 and -3, respectively, spanning 67° S–80° N. On average, consecutive samples in the mid-troposphere are separated by 2.2° of latitude, with 4.4° between consecutive near-surface or high-altitude samples. Most profiles extended from approximately 300 to 8500 m altitude, constrained by air traffic, but significant profiling extended above approximately 14 km (figure 1c).

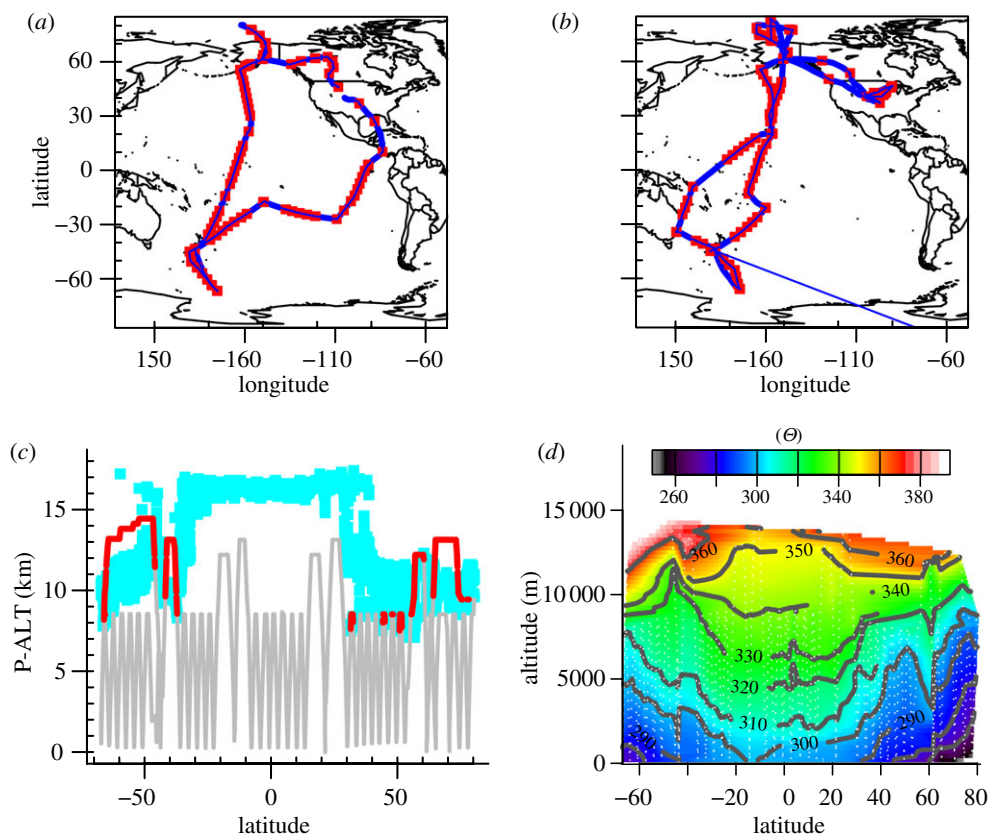


Figure 1. (a, b) Locations of flight tracks and vertical profiles (red points) for HIPPO deployments 1 and 2. (c) Vertical profiles in the HIPPO-1 cross section of the Pacific southbound near the date line (flights 2–7), tropopause heights (pressure altitude (km); cyan) from MTP, and stratospheric flight segments in red. (d) Cross section of potential temperature ( $\Theta$ ) in HIPPO-1, on the southbound leg near the date line. The white dotted lines mark the flight path of the GV, and grey lines show contours of potential temperature. Altitudes are given in metres above sea level (m.a.s.l.) (GPS). (Online version in colour.)

Figure 1d shows the cross section of potential temperature ( $\Theta$ ) versus latitude and GPS altitude (m.a.s.l.) during HIPPO-1. A dome of very cold, stable air, with a strong latitude gradient of  $\Theta$ , covered the Arctic, with a sharp transition at the northern edge of the polar jet, near 60° N. There was a narrow zone of stratospheric influx just equatorward of 60° N, and then a belt of much weaker vertical stratification from 60° to 40° N, the region of the ‘warm conveyor belt’, where vertical transport occurs in association with jet stream dynamics and mid-latitude storms [22,23]. Equatorward of 40° N, there was a broad  $\Theta$  bulge in the middle and upper troposphere, reflecting the influence of deep convection and the Hadley circulation. The Southern Hemisphere (SH) had similar structure, but the features were weaker, reflecting the summer season.

Figure 2 shows cross sections along the date line for key species in January 2009 (HIPPO-1). Atmospheric tracers displayed sharp transitions in the horizontal, demarcating the boundaries between polar, middle latitude, subtropical and

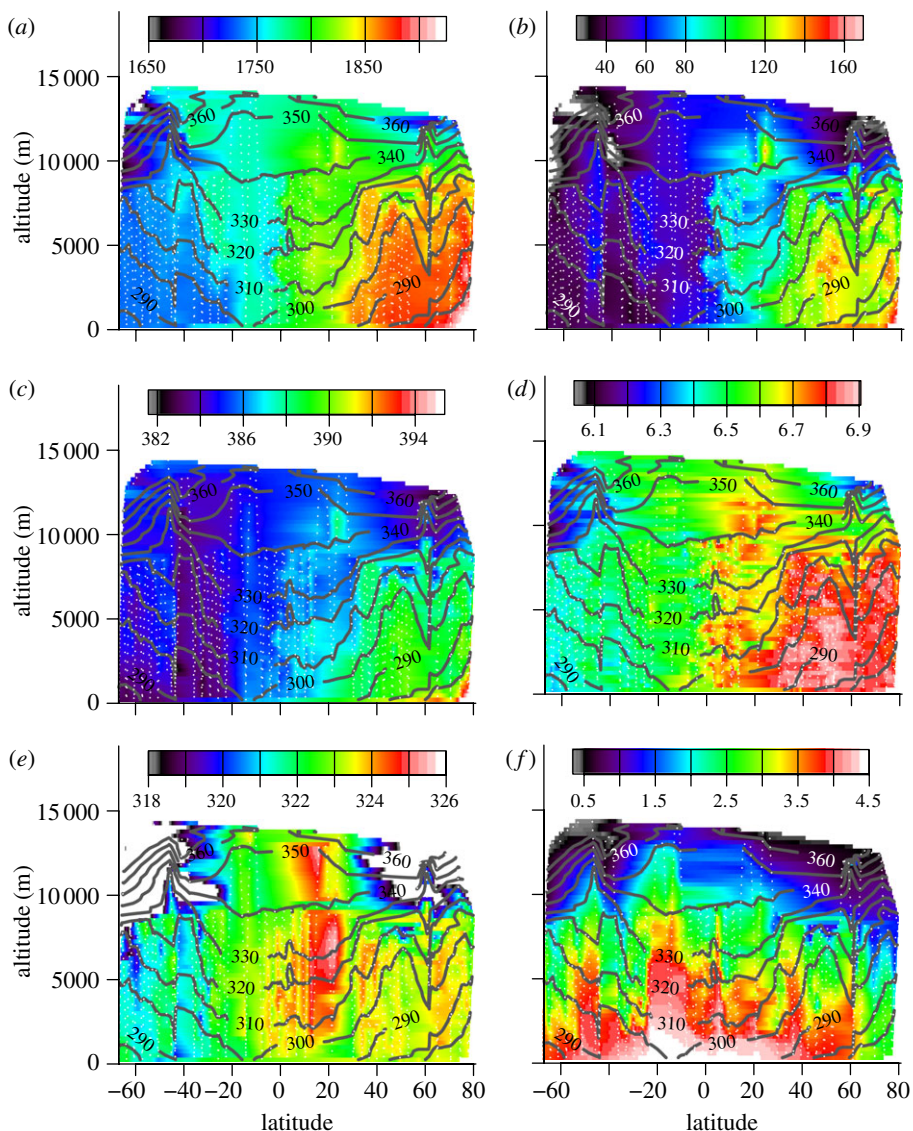


Figure 2. Cross sections of (a) CH<sub>4</sub> (ppb), (b) CO (ppb), (c) CO<sub>2</sub> (ppm), (d) SF<sub>6</sub> (ppt), (e) N<sub>2</sub>O (ppb) and (f) H<sub>2</sub>O (log<sub>10</sub> (ppm)) on HIPPO-1, southbound along the date line, January 2009. White dotted lines show flight tracks, and grey contours show potential temperature. SF<sub>6</sub> data represent a composite of PANTHER and UCATS data, and H<sub>2</sub>O data are from VCSEL. Altitudes are given in m.a.s.l. (GPS). (Online version in colour.)

tropical air masses, and at the intertropical convergence zone (ITCZ; the persistent line of convective storms that circles the globe near the equator, demarcating the boundary between the hemispheres). Gradients were much weaker in the vertical than in the horizontal, except in the northern polar region where fresh inputs of CO, CO<sub>2</sub>, CH<sub>4</sub> and SF<sub>6</sub> were evidenced by high values near the surface and the presence of very short-lived pollutants (e.g.

benzene). According to model simulations (discussed further below), these pollutants originated from Asia and Europe. In the Arctic, tracer isopleths broadly aligned with isentropes, with sporadic anomalies owing to proximate emissions or to stratospheric influence. Convective transport across isentropes was evident elsewhere, in mid-latitudes, tropics and subtropics, particularly for the longest lived tracers (e.g. SF<sub>6</sub> and N<sub>2</sub>O). The peak value of SF<sub>6</sub> over the North Pacific was observed in the middle troposphere. Concentrations of N<sub>2</sub>O showed a completely different pattern from other GHGs, with a prominent bulge in the middle and upper tropical and subtropical troposphere, plus sporadic enhancements between 10 and 14 km. Similar features were seen for N<sub>2</sub>O in all three missions flown so far.

Water vapour showed the expected increases with temperature and tropical origin. Input of very wet air was notable in the South Pacific convergence zone (SPCZ; 10–20° S). The SPCZ is a persistent frontal formation of widespread cloud cover and precipitation extending in a southeast direction from New Guinea into the SH mid-latitudes, with strong convection typically extending over a large area. It is specially prominent in boreal winter [24]. The SPCZ is spatially larger, and contains more intense convection, than similar convergence zones elsewhere, such as the South Indian Convergence Zone (SICZ) and the South Atlantic Convergence Zone (SACZ), although it is not clear why [24]. Analogous, but less distinct, anomalies have been observed for other chemical tracers near the SPCZ [25,26]. In each of the three HIPPO missions so far, the water vapour plume from the SPCZ has been larger in extent, and penetrated deeper into the atmosphere, than in the ITCZ. These results suggest that the SPCZ may be an important global source of water vapour to the tropical tropopause layer over the Pacific, at least in the boreal winter season, supporting inferences from observations of cirrus clouds over the tropical western Pacific during that season [27].

Figure 3 shows cross sections for HIPPO-2 in November 2009. Inverted vertical profiles (i.e. with higher concentrations aloft) were surprisingly strong. Pollutant levels typical of urban corridors were found in a thick layer at 6–8 km over an extensive region of the Arctic, overlying clean air. The layers preserve coherence (figure 3*d,e*) among tracers despite sharp gradients and transport over thousands of kilometres, with strong vertical uplift. Very high levels of BC aerosol were present, and absorption of solar radiation was visible (figure 3*c*). High aerosol concentrations indicate the absence of efficient precipitation scavenging, suggesting that polluted air was lofted by isentropic advection over the cold dome that was in the process of developing over the Arctic. Notable enhancements of N<sub>2</sub>O were observed in some of the plumes. In many descents, enhanced CH<sub>4</sub> concentrations were observed near the surface of the Arctic Ocean, sometimes in otherwise pristine air, possibly signifying emission from biogenic sources or from CH<sub>4</sub> hydrates (e.g. figure 3*c*, below 2000 m). Horizontal gradients were again very sharp at air mass boundaries.

Figure 4 illustrates the meridional gradients of CO<sub>2</sub> and O<sub>2</sub>/N<sub>2</sub>. Concentrations of CO<sub>2</sub> were enhanced above the surface (but not at the surface) from 45° S to 70° S in January (figures 2*c* and 4*a*), which might confirm a signal of elevated CO<sub>2</sub> in this region similar to that reported by the Atmospheric Infrared Sounder (AIRS) satellite [28]; the structure of the CO<sub>2</sub> distribution is rather complex, with probable contributions from multiple processes including fires in Australia

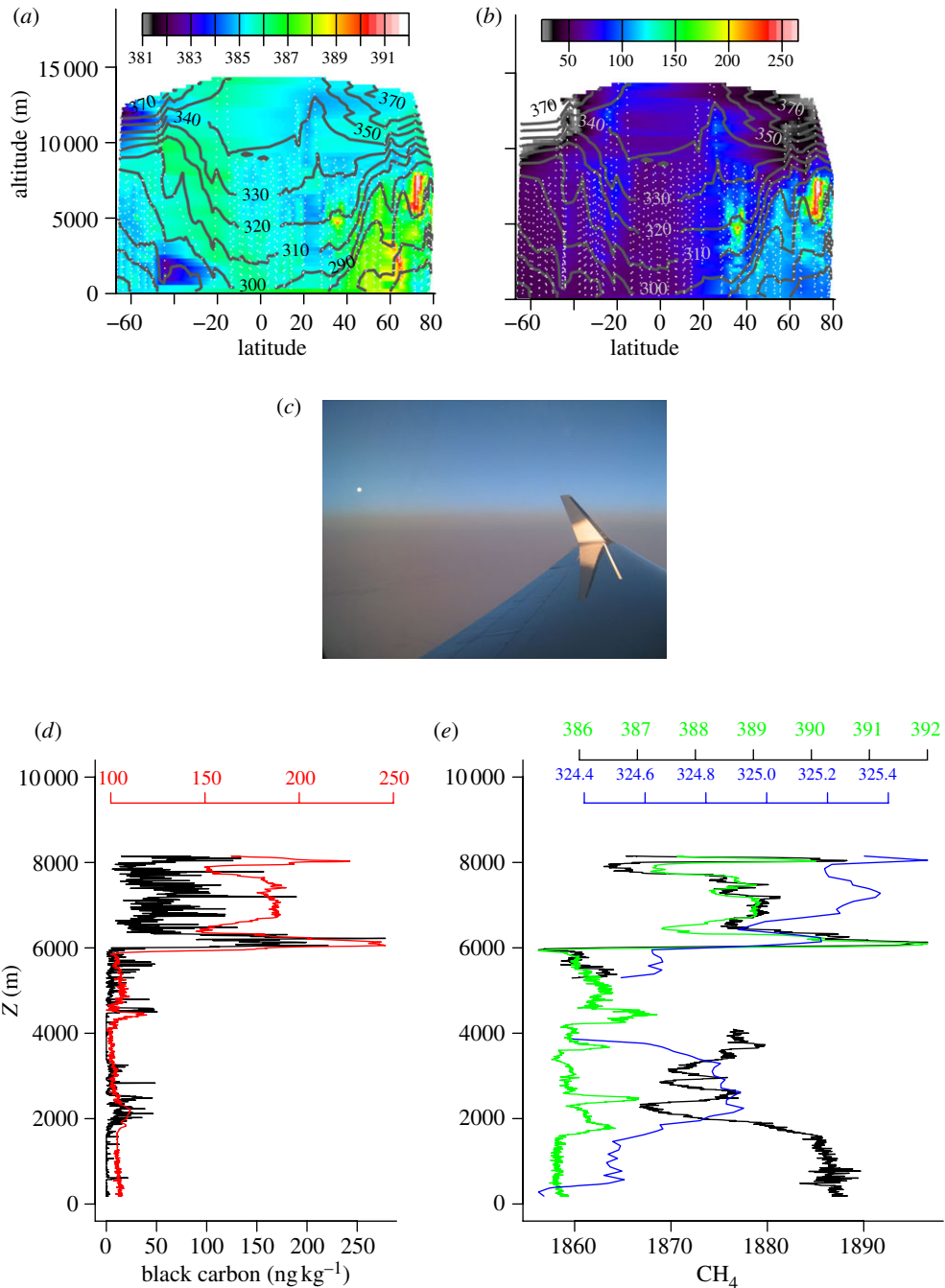


Figure 3. (a, b) Cross sections of CO<sub>2</sub> (ppm) and CO (ppb), on HIPPO-2, southbound along the date line, November 2009. Grey contours show potential temperature. (c) Photo of dense layer of dark aerosols, looking north at 80° N, 8 km altitude, 2 November 2009 (photo: E. Kort). (d) Vertical profiles of black carbon (BC) and CO at 77.2° N, on HIPPO-2, 2 November 2009. Black lines, BC; red lines, CO. (e) Vertical profiles of CO<sub>2</sub>, CH<sub>4</sub> and N<sub>2</sub>O at 77.2° N, on HIPPO-2, 2 November 2009. Black lines, CH<sub>4</sub>; green lines, CO<sub>2</sub>; blue lines, N<sub>2</sub>O. (Online version in colour.)

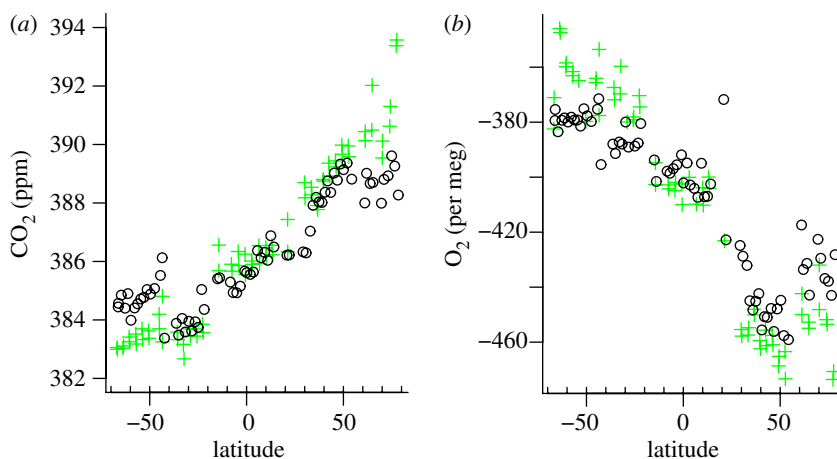


Figure 4. (a) Meridional gradients of CO<sub>2</sub> averaged between 0.3 and 1.5 km and between 3.5 and 6.5 km. (b) Variation of the O<sub>2</sub>:N<sub>2</sub> ratio, as in (a). Green plus symbols, 0.3–1.5 km; open circles, 3.5–6.5 km. (Online version in colour.)

and uptake of CO<sub>2</sub> at the ocean surface. There is excess O<sub>2</sub> near the surface all the way from 20° S to 60° S (figure 4b), reflecting inputs to the atmosphere from both the ocean and the land, including thermal degassing of O<sub>2</sub> from the ocean and biological production of O<sub>2</sub> from land and ocean in summer.

Preliminary simulations of HIPPO-1 data have been made with global models including Goddard Earth Observing System (GEOS) Chemical Tracer Model (CHEM) [1], ACTM [6] and Global and regional Earth-system Monitor using Satellite and in situ data/Monitoring and Forecasting Atmospheric Composition (GEMS/MACC) [29]. Examples are shown in figure 5*a–d*. The models extracted computed values along the flight track for detailed comparison with HIPPO. Model simulations performed reasonably well in many respects, as can be seen by comparing with figure 2. Simulations of CO<sub>2</sub> from the GEOS-CHEM model ([30]; figure 5*a*) captured many features of the observations (figure 2), including the relatively well-mixed profiles in subpolar and middle latitudes. Vertical contrasts occurred mostly over the Arctic and Antarctic/Southern Ocean, reflecting inputs from fossil fuels and marine biological uptake, respectively. But horizontal gradients were much sharper in the atmosphere, and vertical gradients weaker, than in the models. Most satellite data likewise do not resolve the observed gradients. Enhanced CO<sub>2</sub> poleward of 40° S seen by HIPPO is not reproduced in the model; the major pollution signature appears at 60° N instead of 80° N; enhanced surface CO<sub>2</sub> in the SH deep tropics, probably from equatorial upwelling, is not simulated in the model.

Both the ACTM and GEOS-CHEM models appear to have vertical transport rates that are too weak at high latitudes (compare CO<sub>2</sub>, SF<sub>6</sub> and CO in figures 2–5), both along and across isentropes. The GEMS/MACC model gives a somewhat better appearance for vertical profiles of CO and CH<sub>4</sub> (not shown), but has anomalies elsewhere and misses global-scale North–South gradients significantly: GEMS/MACC predicts 70 ppb for ΔCO between the Antarctic and the Arctic, compared with approximately 95 ppb observed.

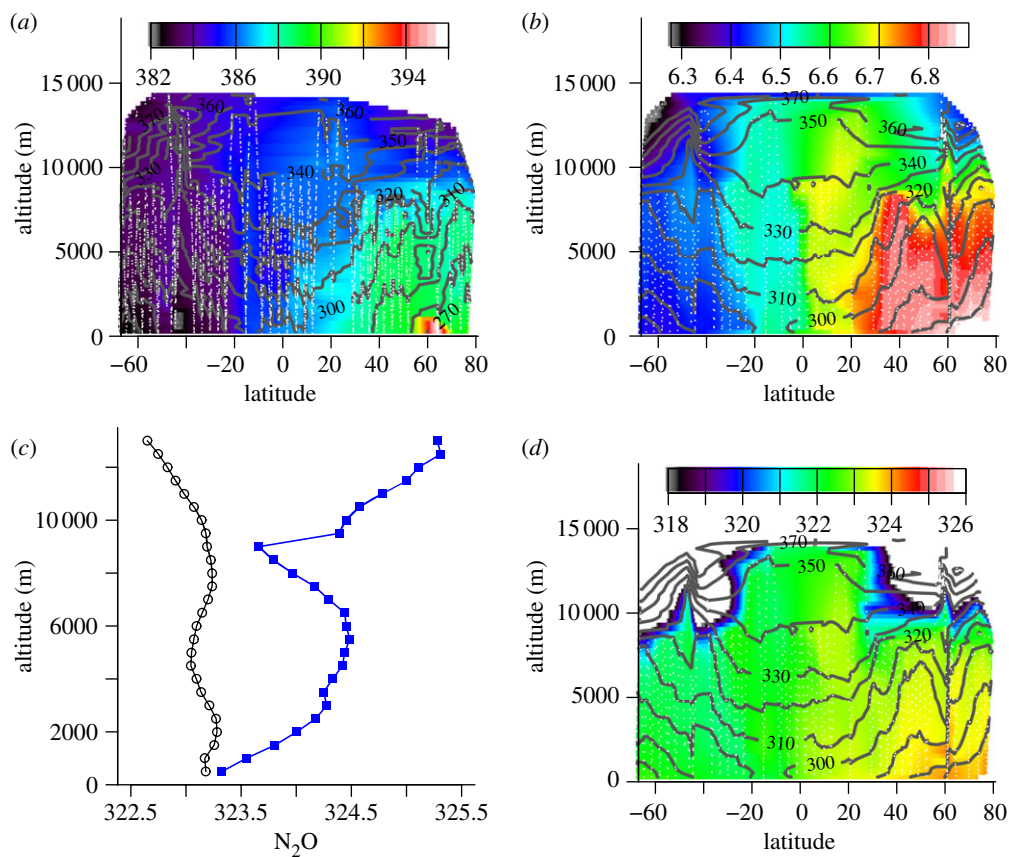


Figure 5. Model simulations for HIPPO-1, southbound along the date line, January 2009. (a,b) Cross sections of CO<sub>2</sub> (ppm) and SF<sub>6</sub> (ppt) from the GEOS-CHEM and ACTM models, respectively. (c) Vertical profiles of N<sub>2</sub>O in the subtropics (ACTM and observed in HIPPO-1). Blue filled squares, HIPPO-1; black open circles, ACTM. (d) Cross section for N<sub>2</sub>O from the ACTM for the HIPPO-1 flight track (flights 2–7). (Online version in colour.)

HIPPO data for N<sub>2</sub>O differ radically from model results. Simulations completely miss the major feature of the global distribution, the tropical/sub-tropical maxima at altitude (figure 5c,d), with greater enhancement north of the ITCZ. This pattern has been observed in all six HIPPO cross sections flown to date, although the magnitude of the enhancement aloft was largest in HIPPO-1 southbound. HYSPLIT [31] trajectories showed that air near the surface originated from the east, whereas the air with enhanced N<sub>2</sub>O concentrations, above 2 km, came from the west, suggesting sources in regions of convection in the western Pacific and/or tropical South Asia or Indonesia. Samples collected on the CARIBIC flights of commercial aircraft from Germany to India [32] also showed diffuse maxima of N<sub>2</sub>O in the upper troposphere (8.5–12 km) during June–August, peaking in the same general latitude range as in HIPPO flights (15–25° N). It appears that much of the excess N<sub>2</sub>O seen by HIPPO was generated in the tropics, but it is difficult to distinguish land-based sources from possible production by corona discharge or lightning in convective storms [33] or by other mechanisms.

Previous studies [34,35] using sparse station data have already suggested that unaccounted tropical sources were needed to close the N<sub>2</sub>O budget. HIPPO data strongly support that view. Elevated concentrations high in the atmosphere found in HIPPO indicate a notably stronger tropical source than could be inferred from surface data only. Even in the north polar region, HIPPO data often showed maximum concentrations of N<sub>2</sub>O aloft (cf. figures 2, 3 and 5), emphasizing the difficulty of using surface measurements for modelling of this important species.

#### 4. Summary and conclusions

HIPPO flights provide a unique dataset for atmospheric research: simultaneous, fine-grained, global, high-frequency measurements of major GHGs, tracers with a wide range of chemical lifetimes and diverse source processes, O<sub>2</sub>/N<sub>2</sub> and Ar/N<sub>2</sub> ratios, BC and aerosols, plus the isotopic composition of CO<sub>2</sub>. Concentration data from HIPPO are linked to world standards, and multiple measurements provide checks on data quality. The data from all missions will be publicly available within 12–18 months of collection. HIPPO data have already played a major role in calibrating total column measurements of CO<sub>2</sub>, CO and CH<sub>4</sub> from the Total Carbon Column Observing Network (TCCON) of Fourier transform spectrometers [36].

First impressions already highlight new phenomena: dense pollution high over the Arctic in late autumn/early winter, with a notable component of BC; the imprint of large N<sub>2</sub>O sources in the tropical or subtropical areas of Asia or the western Pacific and sources of CH<sub>4</sub> in the Arctic both from fossil-fuel extraction and from non-industrial sources. Although not discussed here, we also observed short-lived gases emanating from various marine environments across the Pacific (e.g. methyl nitrate, haloforms) and from major industrial areas.

HIPPO data clearly delineate the atmospheric imprint of summertime sinks for CO<sub>2</sub> and sources for O<sub>2</sub> in the SH, providing a new tool to infer the strength of ocean and land fluxes in the carbon cycle. Curtain plots reveal large-scale features invisible to satellites and blurred by models, revealing the internal structure of global CO<sub>2</sub> distributions hitherto observed fuzzily by satellites and sparse remote stations.

The most novel aspect of HIPPO is the imaging of the signatures of global atmospheric transport modes with high clarity. From the SPCZ and ITCZ to the cold dome over the winter pole, HIPPO data show the influence of convection, isentropic transport and stratosphere–troposphere exchange, with fine resolution at global scale. Remarkably sharp gradients in tracer concentrations are observed at air mass boundaries. Inverted tracer gradients, with maxima aloft, were found to be common in both hemispheres over the Pacific. These features present major challenges to global models and to observation systems using sparse surface stations and satellites. If not represented in global inverse model studies, they can lead to major biases and inconsistencies. HIPPO data can play a crucial role in identifying and resolving these issues.

The HIPPO Programme was supported by NSF grants ATM-0628575, ATM-0628519 and ATM-0628388 to Harvard University, University of California (San Diego), University Corporation for Atmospheric Research, University of Colorado/CIRES and by the NCAR. The NCAR is supported by the National Science Foundation. Participation by several instruments (SP-2, Ozone, UCATS,

PANTHER, NWAS flasks), and weather forecasting, were supported by offices and programmes of the National Oceanic and Atmospheric Administration: the Atmospheric Composition and Climate Programme, the Office of Oceanic and Atmospheric Research and the Environmental Research Laboratory. The AWAS flasks system was supported by NSF grants NSF ATM0849086 and AGS0959853 to the University of Miami. VCSEL was supported by NSF grant AGS-1036275 to Princeton University. We are grateful to the crew of the GV for their dedication and professional skill in making the flights possible and in taking the GV to places not previously visited by a jet aircraft, and to the NCAR Earth Observing Laboratory for support of logistics and public outreach. The authors gratefully acknowledge the NOAA Air Resources Laboratory (ARL) for the provision of the HYSPLIT transport and dispersion model.

<sup>†</sup>S. C. Wofsy, B. C. Daube, R. Jimenez, E. Kort, J. V. Pittman, S. Park, R. Commane, B. Xiang, G. Santoni, D. Jacob, J. Fisher, C. Pickett-Heaps, H. Wang, K. Wecht, Q.-Q. Wang (School of Engineering and Applied Science, Harvard University, Cambridge, MA, USA); B. B. Stephens, S. Shertz, P. Romashkin, T. Campos, J. Haggerty, W. A. Cooper, D. Rogers, S. Beaton, R. Hendershot (National Center for Atmospheric Research, Boulder, CO, USA); J. W. Elkins, D. W. Fahey, R. S. Gao, F. Moore, S. A. Montzka, J. P. Schwarz, D. Hurst, B. Miller, C. Sweeney, S. Oltmans, D. Nance, E. Hints, G. Dutton, L. A. Watts, J. R. Spackman, K. H. Rosenlof, E. A. Ray, B. Hall (NOAA ESRL and CIRES, Boulder, CO, USA); M. A. Zondlo, M. Diao (Department of Civil and Environmental Engineering, Princeton University, Princeton, NJ, USA); R. Keeling, J. Bent (Scripps Institution of Oceanography, University of California at San Diego, CA, USA); E. L. Atlas, R. Lueb (Rosensiel School of Marine and Atmospheric Science, University of Miami, Miami, FL, USA); M. J. Mahoney, M. Chahine, E. Olsen (Jet Propulsion Laboratory, Pasadena, CA, USA); P. Patra, K. Ishijima (Research Institute for Global Change, JAMSTEC, Yokohama, Japan); R. Engelen, J. Flemming (European Centre for Medium-Range Weather Forecasts, Reading, UK); R. Nassar, D. B. A. Jones (Department of Physics, University of Toronto, Toronto, Canada); S. E. Mikaloff Fletcher (National Institute for Water and Atmospheric Research, Wellington, New Zealand).

## References

- 1 Bey, I. *et al.* 2001 Global modeling of tropospheric chemistry with assimilated meteorology: model description and evaluation. *J. Geophys. Res. Atmos.* **106**, 23 073–23 095. (doi:10.1029/2001JD000807)
- 2 Engelen, R. J., Serrar, S. & Chevallier, F. 2009 Four-dimensional data assimilation of atmospheric CO<sub>2</sub> using AIRS observations. *J. Geophys. Res.* **114**, D03303. (doi:10.1029/2008JD010739)
- 3 Gurney, K. R. *et al.* 2002 Towards robust regional estimates of CO<sub>2</sub> sources and sinks using atmospheric transport models. *Nature* **415**, 626–630. (doi:10.1038/415626a)
- 4 Kort, E. A. *et al.* 2008 Emissions of CH<sub>4</sub> and N<sub>2</sub>O over the United States and Canada based on a receptor-oriented modeling framework and COBRA-NA atmospheric observations. *Geophys. Res. Lett.* **35**, L18808. (doi:10.1029/2008GL034031)
- 5 Michalak, A. M., Bruhwiler, L. & Tans, P. P. 2004 A geostatistical approach to surface flux estimation of atmospheric trace gases. *J. Geophys. Res. Atmos.* **109**, D14109. (doi:10.1029/2003JD004422)
- 6 Patra, P. K., Takigawa, M., Dutton, G. S., Uhse, K., Ishijima, K., Lintner, B. R., Miyazaki, K. & Elkins, J. W. 2009 Transport mechanisms for synoptic, seasonal and interannual SF<sub>6</sub> variations and ‘age’ of air in troposphere. *Atmos. Chem. Phys.* **9**, 1209–1225. (doi:10.5194/acp-9-1209-2009)
- 7 Ishijima, K. *et al.* 2010 The stratospheric influence on the seasonal cycle of nitrous oxide in the troposphere, deduced from aircraft observations and model simulations. *J. Geophys. Res.* **115**, D20308. (doi:10.1029/2009JD013322)
- 8 Pan, L. L. *et al.* 2010 The stratosphere–troposphere analyses of regional transport 2008 experiment. *Bull. Am. Meteorol. Soc.* **91**, 327–342. (doi:10.1175/2009BAMS2865.1)

- 9 Rastigejev, Y., Park, R., Brenner, M. P. & Jacob, D. J. 2010 Resolving intercontinental pollution plumes in global models of atmospheric transport. *J. Geophys. Res.* **115**, D02302. (doi:10.1029/2009JD012568)
- 10 Stephens, B. B. *et al.* 2007 Weak northern and strong tropical land carbon uptake from vertical profiles of atmospheric CO<sub>2</sub>. *Science* **316**, 1732–1735. (doi:10.1126/science.1137004)
- 11 Machida, T. *et al.* 2008 Worldwide measurements of atmospheric CO<sub>2</sub> and other trace gas species using commercial airlines. *J. Atmos. Ocean. Technol.* **25**, 1744–1754. (doi:10.1175/2008JTECHA1082.1)
- 12 Nakazawa, T., Miyashita, K., Aoki, S. & Tanaka, M. 1991 Temporal and spatial variations of upper tropospheric and lower stratospheric carbon dioxide. *Tellus B* **43**, 106–117. (doi:10.1034/j.1600-0889.1991.t01-1-00005.x)
- 13 Marengo, A. *et al.* 1998 Measurement of ozone and water vapor by Airbus in-service aircraft: the MOZAIC airborne program—an overview. *J. Geophys. Res. Atmos.* **103**, 25 631–25 642. (doi:10.1029/98JD00977)
- 14 Davis, D. D. 1980 Project gametag—an overview. *J. Geophys. Res. Oceans Atmos.* **85**, 7285–7292. (doi:10.1029/JC085iC12p07285)
- 15 Hoell, J. M., Davis, D. D., Jacob, D. J., Rodgers, M. O., Newell, R. E., Fuelberg, H. E., McNeal, R. J., Raper, J. L. & Bendura, R. J. 1999 The Pacific exploratory mission in the tropical Pacific: PEM-tropics A, August–September 1996. *J. Geophys. Res.* **104**, 5567–5584. (doi:10.1029/1998JD100074)
- 16 Jacob, D. J. *et al.* 2003 The transport and chemical evolution over the Pacific (TRACE-P) aircraft mission: design, execution, and first results. *J. Geophys. Res.* **108**, 9000. (doi:10.1029/2002JD003276)
- 17 Raper, J. L., Kleb, M. M., Jacob, D. J., Davis, D. D., Newell, R. E., Fuelberg, H. E., Bendura, R. J., Hoell, J. M. & McNeal, R. J. 2001 Pacific exploratory mission in the tropical Pacific: PEM-tropics B, March–April 1999. *J. Geophys. Res.* **106**, 32 401–32 425. (doi:10.1029/2000JD900833)
- 18 Daube, B. C., Boering, K. A., Andrews, A. E. & Wofsy, S. C. 2002 A high-precision fast-response airborne CO<sub>2</sub> analyzer for *in situ* sampling from the surface to the middle stratosphere. *J. Atmos. Ocean. Technol.* **19**, 1532–1543. (doi:10.1175/1520-0426(2002)019<1532:AHPFRA>2.0.CO;2)
- 19 Zondlo, M. A., Paige, M. E., Massick, S. M. & Silver, J. A. 2010 Development, flight performance, and calibrations of the NSF Gulfstream-V vertical cavity surface emitting laser (VCSEL) hygrometer. *J. Geophys. Res. Atmos.* **115**, D20309. (doi:10.1029/2010JD014445)
- 20 Stephens, B. B., Keeling, R. F. & Paplawsky, W. J. 2003 Shipboard measurements of atmospheric oxygen using a vacuum-ultraviolet absorption technique. *Tellus B Chem. Phys. Meteorol.* **55**, 857–878. (doi:10.1046/j.1435-6935.2003.00075.x)
- 21 Schwarz, J. P. *et al.* 2008 Coatings and their enhancement of black-carbon light absorption in the tropical atmosphere. *J. Geophys. Res.* **113**, D03203. (doi:10.1029/2007JD009042)
- 22 Bethan, S., Vaughan, G., Gerbig, C., Volz-Thomas, A., Richer, H. & Tiddeman, D. A. 1998 Chemical air mass differences near fronts. *J. Geophys. Res.* **103**, 13 413–13 434. (doi:10.1029/98JD00535)
- 23 Cooper, O. R. *et al.* 2004 A case study of transpacific warm conveyor belt transport: influence of merging airstreams on trace gas import to North America. *J. Geophys. Res.* **109**, D23S08. (doi:10.1029/2003JD003624)
- 24 Widlansky, M. 2007 Variability of the South Pacific convergence zone and its influence on the general atmospheric circulation. Masters thesis, Georgia Institute of Technology, USA, p. 76.
- 25 Gregory, G. L. *et al.* 1999 Chemical characteristics of the Pacific tropospheric air in the region of the intertropical convergence zone and South Pacific convergence zone. *J. Geophys. Res.* **104**, 5677–5696. (doi:10.1029/98JD01357)
- 26 Mari, C. *et al.* 2003 On the relative role of convection, chemistry, and transport over the South Pacific convergence zone during PEM-tropics B: a case study. *J. Geophys. Res. Atmos.* **108**, 8232. (doi:10.1029/2001JD001466)
- 27 Fujiwara, M. *et al.* 2009 Cirrus observations in the tropical tropopause layer in the western Pacific. *J. Geophys. Res. Atmos.* **114**, D09304. (doi:10.1029/2008JD011040)

- 28 Chahine, M. T., Chen, L., Dimotakis, P., Jiang, X., Li, Q., Olsen, E. T., Pagano, T., Randerson, J. & Yung, Y. L. 2008 Satellite remote sounding of mid-tropospheric CO<sub>2</sub>. *Geophys. Res. Lett.* **35**, L17807. (doi:10.1029/2008GL035022)
- 29 Hollingsworth, A. *et al.* & the GEMS consortium. 2009 Toward a monitoring and forecasting system for atmospheric composition. The GEMS project. *Bull. Am. Meteorol. Soc.* **89**, 1147–1164. (doi:10.1175/2008BAMS2355.1)
- 30 Nassar, R. *et al.* 2010 Modeling global atmospheric CO<sub>2</sub> with improved emission inventories and CO<sub>2</sub> production from the oxidation of other carbon species. *Geosci. Model Dev. Discuss.* **3**, 889–948. (doi:10.5194/gmdd-3-889-2010)
- 31 Draxler, R. R. & Rolph, G. D. 2010 *HYSPLIT (Hybrid Single-Particle Lagrangian Integrated Trajectory) Model access via NOAA ARL READY*. Silver Spring, MD: NOAA Air Resources Laboratory. See <http://ready.arl.noaa.gov/HYSPLIT.php>.
- 32 Schuck, T. J., Brenninkmeijer, C. A. M., Baker, A. K., Slemr, F., von Velthoven, P. F. J. & Zahn, A. 2010 Greenhouse gas relationships in the Indian summer monsoon plume measured by the CARIBIC passenger aircraft. *Atmos. Chem. Phys.* **10**, 3965–3984. (doi:10.5194/acp-10-3965-2010)
- 33 Martinez, P. & Brandvold, D. K. 1996 Laboratory and field measurements of NO<sub>x</sub> produced from corona discharge. *Atmos. Environ.* **30**, 4177–4182. (doi:10.1016/1352-2310(96)00156-2)
- 34 Hirsch, A. I., Michalak, A. M., Bruhwiler, L. M., Peters, W., Dlugokencky, E. J. & Tans, P. P. 2006 Inverse modeling estimates of the global nitrous oxide surface flux from 1998–2001. *Glob. Biogeochem. Cycles* **20**, GB1008. (doi:10.1029/2004GB002443)
- 35 Huang, J. *et al.* 2008 Estimation of regional emissions of nitrous oxide from 1997 to 2005 using multinetwork measurements, a chemical transport model, and an inverse method. *J. Geophys. Res.* **113**, D17313. (doi:10.1029/2007JD009381)
- 36 Wunch, D. *et al.* 2010 Calibration of the total carbon column observing network using aircraft profile data. *Atmos. Meas. Tech. Discuss.* **3**, 2603–2632. (doi:10.5194/amtd-3-2603-2010)